

# Robustness of ballistic transport features in antidot superlattices

George Datsaris,\* Theo Geisel, and Ragnar Fleischmann  
Max Planck Institute for Dynamics and Self-Organization  
(Dated: Saturday 14<sup>th</sup> December, 2024)

The magneto-resistance of antidot lattices shows pronounced peaks, which became a hallmark of ballistic electron transport. While most studies agree that they reflect the interplay of regular and chaotic motion in the quasi-classical dynamics, the exact mechanism has been surprisingly controversial. Inspired by recent experiments on graphene antidot lattices showing that the effect survives strong impurity scattering, we give a new explanation of the peaks linked to a fundamental relation between collision times and accessible phase space volumes, accounting for their robustness.

Antidot superlattices are nanostructured artificial crystals of repellers in high mobility two-dimensional electron gases (2DEGs). They were first fabricated by ion-beam implantation [1] or etching periodic arrays of holes with periods of a few hundred nanometers into the 2DEG of AlGaAs/GaAs heterostructures [2] and by modulation of the 2DEG by nanostructured lateral metal gates [3]. Since then antidots were realized in many different materials [4] and recently also in graphene [5, 6]. They are a prime example of devices showing features of ballistic transport: when the typical length scales of a device become smaller than the mean free path of the electrons, transport is no longer dominated by diffusion due to impurity, phonon or electron-electron scattering. Instead, transport is mainly affected by external forces or the potential of the device superstructure. The most prominent of a number of ballistic transport effects observed in antidot lattices is their low temperature magneto-resistance at small magnetic fields which typically shows a series of pronounced peaks. It was realized [2] that they occur at magnetic field values where collision-less circular cyclotron orbits encircling a certain numbers of antidots can exist in the superlattice (see e.g. Figs. 1, 2) and they are therefore known as *commensurability peaks* (CPs). At even lower temperatures, when the coherence length of the electrons grows, quantization of periodic orbits manifests itself in additional resistivity oscillations [7–9]. In the following we will consider the *incoherent* ballistic transport, which can be analyzed in terms of quasi-classical dynamics [10]. Such quasi-classical resistivity peaks have even been observed at high magnetic fields in the fractional quantum hall regime, where compound quasi-particles, so called *composite fermions*, experience a reduced effective magnetic field [11, 12].

While most studies agree that the CPs reflect the interplay of regular and chaotic quasi-classical dynamics, their origin has remained controversial [10, 13–16]. Recent experiments by Sandner *et al.* [5] on antidot lattices in monolayer graphene can give us new insight, as they reveal the existence of CPs despite strong impurity scattering. In the present letter we analyze the quasi-classical

electron dynamics in graphene antidot lattices to interpret these magnetoresistance experiments and provide a new explanation for the mechanisms giving rise to CPs in general.

The first attempt to explain CPs was based on the assumption that cyclotron orbits encircling antidots get *pinned* by the antidots and do not contribute to conduction [2]. It was shown theoretically that nonlinear resonances in soft wall models can give rise to such a pinning mechanism [10]. Furthermore it was demonstrated that the resistivity contributions of the chaotic (i.e. non pinned) trajectories alone can already produce CPs and that pinning is not the dominant effect [10]. How the chaotic dynamics leads to CPs, however, was strongly disputed (see e.g. [10, 13–16]). In any case one would assume that the mean impurity scattering time  $\tau_i$  due to residual disorder in the substrate must be sufficiently long in order to observe features of chaotic ballistic dynamics and nonlinear resonances in transport measurements. More specifically it should fulfill  $\omega\tau_i \gg 2\pi$ , where  $\omega$  is the typical frequency of the nonlinear resonances (which is on the order of the cyclotron frequency  $\omega_c$ ). In the graphene experiments by Sandner *et al.* [5] and Yagi *et al.* [6], however, the scattering time is short and  $\omega\tau_i \lesssim 1$ . Why do the experiments still exhibit CPs nevertheless? In this letter we will show that the resistance peaks survive the impact of these short impurity scattering times, because the fast chaotic time scale, the mean time between (successive) collisions with antidots, is reduced by the mere existence of nonlinear resonances as they are taking away chaotic phase space volume. Our analysis gives a simple and very general explanation of the phenomenon, which will be applicable to a wide range of billiard-like mesoscopic systems, since the intrinsic scattering time of the chaotic orbits is generally linked to the nonlinear resonances simply by their phase space volume.

We model the conduction electrons by a quasi-classical micro-canonical ensemble at the Fermi energy  $E_F$ . As we want to describe graphene experiments, we obtain the kinetic energy term from the dispersion relation by substituting  $\hbar\mathbf{k} \rightarrow \mathbf{p}$ . In the Dirac approximation the dispersion relation of graphene is  $\epsilon(\mathbf{k}) = v_F\hbar|\mathbf{k}|$  (with the Fermi velocity  $v_F \approx 10^6\text{m/s}$ ). Thus, the kinetic

\* george.datsaris@ds.mpg.de

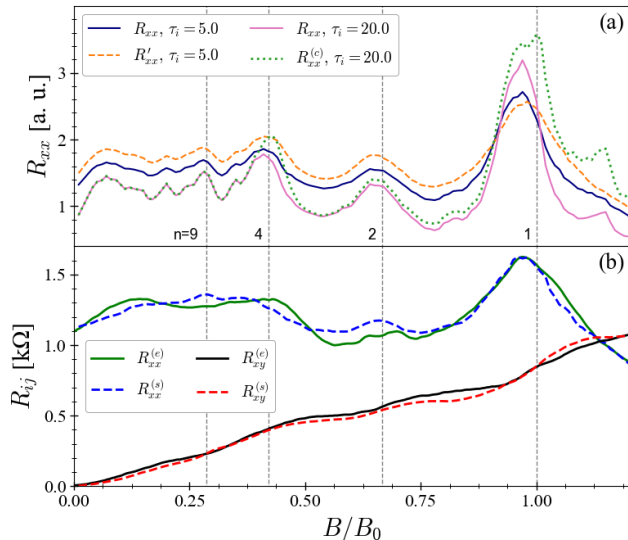


FIG. 1. (a): Magneto-resistance simulations in a steep potential ( $c = 0.1, d = 0.3$ ) for two different  $\tau_i$ .  $R'_{xx}$  denotes simulations with boundary roughness (see Fig. 2b).  $R^{(c)}$  is the resistivity of the chaotic part of the phase space. Vertical dashed lines indicate the commensurable fields  $B_n$  (compare Fig. 2). (b) Comparison of recent experiments  $R^{(e)}$  by Sandner *et al.* [5] with simulations  $R^{(s)}$  using parameters  $c = 0.2$ ,  $d_0 = 0.3, \tau_i = 2.5$  and  $B_0 = 3.7$  T (the prefactor was determined by a least squares fit).

energy becomes  $v_F \sqrt{p_x^2 + p_y^2}$ . The magnetic field perpendicular to the graphene layer is introduced by *minimal coupling*,  $\mathbf{p} \rightarrow \mathbf{p} - e\mathbf{A}$ , choosing the vector potential  $\mathbf{A} = -\frac{1}{2}\mathbf{r} \times \mathbf{B} = \frac{1}{2}(-yB, xB, 0)$ . We model the antidot superlattice by a square array of localized, isotropic potential peaks of the form  $U = \left(\frac{E_F}{c^4}\right) \left[\frac{d_0}{2} + c - r\right]^4$  if  $r = \sqrt{(x - x_a)^2 + (y - y_a)^2} < \frac{d_0}{2} + c$  and 0 otherwise.  $(x_a, y_a)$  is the center of the nearest antidot,  $d_0$  is the antidot diameter (in the experiment by Sandner *et al.* [5] reported values are  $d_0 \approx 25 - 30$  nm with antidot spacing  $a \approx 100$  nm). A contour plot is given in Fig. 2. The parameter  $c$  defines a cut-off distance of the potential and also controls the steepness of the antidots. Details of the potential shape do not play an important role however. Even though the diameter and smoothness of the antidots are important parameters, different functional forms of the potential (e.g. cos, like in [10]) seem to have little impact on the resistivities and no bearing at all on our main conclusions, as will become clear below. Similarly different kinetic energy terms, e.g.  $\epsilon(\mathbf{k}) \sim \mathbf{k}^2$ , do not lead to qualitative changes.

Introducing dimensionless variables  $x_i \rightarrow x_i/a$ ,  $v_i \rightarrow v_i/v_F$  and scaling the energy by the Fermi energy  $E_F = \hbar v_F \sqrt{\pi n_e}$  ( $\approx 0.1 - 1$  eV for the electron densities  $n_e$  re-

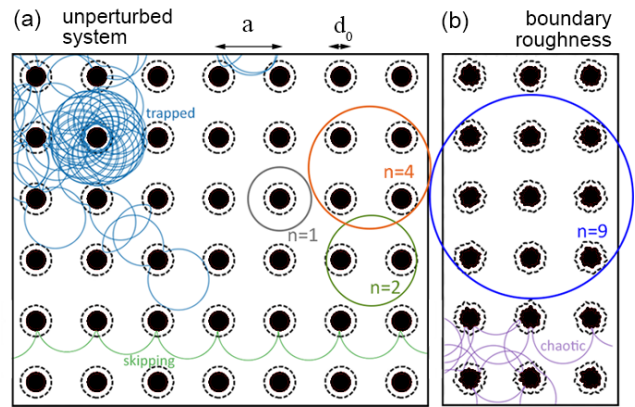


FIG. 2. Plot of the potential  $U$  (filled contours:  $U \geq 1$ , dashed lines:  $U = 0$ ). Antidots with boundary roughness are shown in (b). Examples of chaotic, skipping, and trapped orbits at  $B = 1.0$  and pinned orbits enclosing  $n = 1, 2, 4$  and  $9$  antidots at the commensurable fields  $B_n \in \{1, 0.66, 0.42, 0.285\}$  are shown in various colors.

ported in [5]), the Hamiltonian of our model becomes

$$\mathcal{H} = 1 = \sqrt{(p_x + yB)^2 + (p_y - xB)^2} + \mathcal{U}(x, y). \quad (1)$$

We scale the magnetic field by its value at the principal ( $n = 1$ ) commensurability  $B_0 = 2\hbar\sqrt{\pi n_e}/(ea)$ , corresponding to a cyclotron diameter equaling the antidot lattice constant  $a$ . All times are given in units of  $t_0 = a/v_F$  and the cyclotron frequency is  $\omega_c = 2B$ .

We calculate the conductivities  $\sigma_{ij}$  ( $ij = xx$  or  $xy$ ) and the magneto- and Hall-resistivity  $R_{xx}$  and  $R_{xy}$ , using the Kubo formalism following [10]:

$$\sigma_{ij} \sim \int_0^\infty e^{-t/\tau_i} \langle v_i(t)v_j(0) \rangle_{E_F} dt, \quad (2)$$

$$R_{ij} = \frac{\sigma_{ij}}{\sigma_{xx}^2 + \sigma_{xy}^2}. \quad (3)$$

$C_{ij}(t) \equiv \langle v_i(t)v_j(0) \rangle_{E_F}$  is the (equilibrium) velocity correlation function (VCF) at the Fermi energy. Equation (2) includes impurity scattering using the assumption that the electron velocities are decorrelated by random scattering events. Thus, for events following a Poisson process with mean  $\tau_i$ , the VCFs are weighted with the survival probability  $\exp(-t/\tau_i)$  [17]. In the experiments, the authors estimated  $\tau_i \approx 3.5$  [5]. In the absence of the antidot potential Eqs. (2) and (3) recover the classical Drude result.

The electron dynamics in antidot superlattices in transverse magnetic fields has the *mixed phase-space* structure of generic chaotic Hamiltonian systems: nonlinear resonances form *stable islands* of regular motion in a *chaotic sea* of irregular dynamics. It is useful to divide the VCFs into two contributions: the decaying correlations  $C_{ij}^{(c)}$  of the ergodic chaotic sea with relative

phase space measure  $g_c$  and the non-decaying correlations  $C_{ij}^{(r)}$  of the regular phase space regions with total relative measure  $g_r$ , where  $g_c + g_r = 1$ . We thus write  $C_{ij} = (1 - g_c)C_{ij}^{(r)} + g_c C_{ij}^{(c)}$ , and subsequently

$$\sigma_{ij} = (1 - g_c)\sigma_{ij}^{(r)} + g_c \sigma_{ij}^{(c)} \quad (4)$$

Part of the stable islands correspond to almost circular periodic (or quasi-periodic) orbits, which in a smooth antidot potential are stable against the application of an external electric field [10] and which are therefore called *pinned* orbits. Examples of these orbits at the first four commensurabilities are shown in Fig. 2. Other islands correspond to various forms of *skipping* (also called *run-away* [13]) orbits, an example is also shown in the figure. It has been argued that this kind of skipping orbits may be important for the creation of resistance peaks [13–16]. *Boundary roughness*, which probably is present in the experiments of Ref. [5], however, destabilizes them. As it will become clear below that the formation of the peaks actually does not rely on the presence of this kind of orbits, we will not discuss them further. We model boundary roughness by introducing fluctuating angle dependent antidot diameters  $d(\phi)$  with  $\langle d(\phi) \rangle_\phi = d_0$ , as illustrated in Fig. 2b.

Figure 1a shows example magneto-resistivity curves for the unperturbed antidot lattice for two values of the impurity scattering time  $\tau_i = 5, 20$ . An excellent fit to the experiment in magneto- and Hall-resistivity is achieved for a small scattering time  $\tau_i = 2.5$ , as shown in panel b. Since in the experiments  $\tau_i$  is smaller than  $2\pi/\omega_c$ , we cannot assume that the regular orbits are actually pinned (with  $\sigma_{ij}^{(r)} = 0$  as in Ref. [10]), as they get scattered before they close. We therefore treated them within the Kubo formalism. They lead to Drude like contributions with  $C_{xx}^{(r)}(t) \approx \cos(2Bt)/2$  and  $C_{xy}^{(r)}(t) \approx \sin(2Bt)/2$ .

The magneto-resistance of an antidot lattice with boundary roughness ( $R'_{xx}$ ), shown in Fig. 1a exhibits surprisingly little differences from the unperturbed lattice, confirming that skipping orbits do not strongly contribute to the CPs. On the other hand, the resistivity curve  $R_{xx}^{(c)}$  of the chaotic part of the phase space only, obtained by inverting  $\sigma_{ij}^{(c)}$ , also fully reveals all CPs already. It thus suffices to understand how the chaotic correlations vary with the magnetic field to produce CPs.

Chaotic orbits get *trapped* by nonlinear resonances [10, 18], i.e. they follow the quasiperiodic motion of the resonance for long times, as illustrated in Fig. 2a in light blue color. This leads to slowly decaying correlations of the chaotic orbits. It was therefore argued that it should give rise to valleys rather than peaks in the magneto-resistance [15]. We will show, however, that this effect is overcompensated by an initially enhanced correlation decay as a direct consequence of phase space volume conservation.

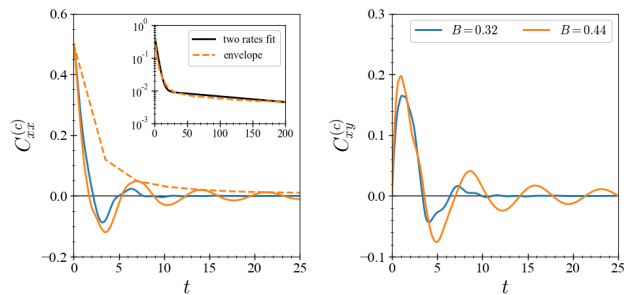


FIG. 3. Velocity correlations of chaotic orbits for  $B = 0.32, 0.44$ . The dashed line shows the envelope of  $C_{xx}^{(c)}$  at the  $n = 4$  commensurability. The inset shows that it is well approximated by two distinct exponential decay rates.

To do so, let us first inspect examples of the chaotic VCFs  $C_{ij}^{(c)}(t)$  in Fig. 3. In the absence of stable islands in phase space ( $B = 0.32$ ) we observe a single rapid correlation decay. In the presence of nonlinear resonances ( $B = 0.44$ ), we see slowly decaying correlation functions due to trapping. From the inset however, which shows the envelope of the autocorrelation, it becomes clear, that the decay is an overlap of a fast and a slow component. We may think of it in the form

$$C_{xx}^{(c)} \approx g_{\text{col}} C_{\text{fast}}(t) + g_{\text{trap}} C_{\text{slow}}(t) \quad (5)$$

where  $g_{\text{trap}}$  is an appropriate measure of the trapping regions in the chaotic sea, and  $g_{\text{col}} = g_c - g_{\text{trap}}$  is its complement, i.e. the phase space region with strong chaotic scattering at the antidots (“*collisions*”). The black dotted line illustrates this division by fitting exponential correlation decays with a fast and a slow time constant,  $\tau_{\text{fast}} \approx 3.5$  and  $\tau_{\text{slow}} \approx 250$ , with  $g_{\text{trap}} \approx 2\%$ . At this point, the detailed values do not matter. What we see is that  $\tau_{\text{slow}}$  is orders of magnitude larger than  $\tau_i$ . The slow decay rate is therefore almost zero in comparison and the portion of trapped chaotic orbits is just a small correction to the portion of pinned orbits. The main contribution to the CPs stems from the change in the fast decay. This can be studied best in a billiard model with infinitely steep antidot walls, which should be a good approximation for these highly chaotic trajectories.

In the remainder of this letter we will therefore study the periodic (or extended) *Sinai billiard* (PSB) [19], also called *periodic Lorentz gas*, as in Ref. [2]. The PSB is probably the most prominent example of a low-dimensional ergodic system [20] and could have been our primary model on its own right, but it does not agree with the experiments just as well. We denote the collision times in the PSB by  $t_\kappa$  and the mean collision time by  $\kappa$ , having in mind that the time scale of the fast correlation decay  $\tau_{\text{fast}}$  in the original model is approximated by  $\kappa$ .

Figure 4a shows  $\kappa$  as a function of the magnetic field.

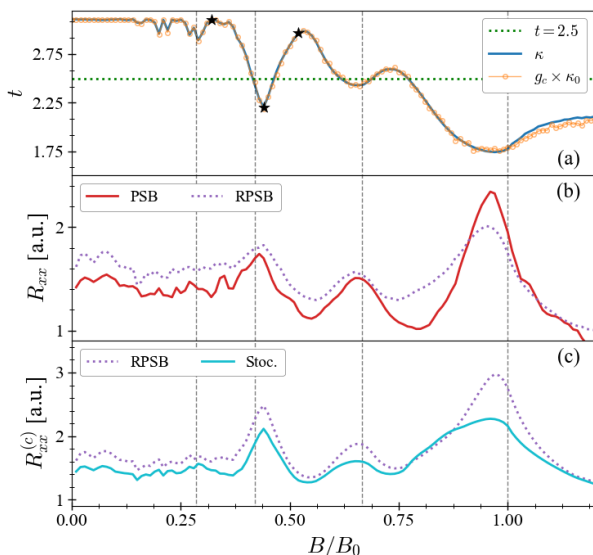


FIG. 4. (a): Average collision time  $\kappa$  in the periodic Sinai billiard (PSB) versus the magnetic field  $B$ , compared to the portion of chaotic orbits  $g_c$  in the PSB, multiplied with  $\kappa$  at 0 field. (b) Resistivity curves of the PSB and rough-PSB. (c) Comparison of the resistivity of the chaotic orbits with the stochastic model (labeled “Stoc.”). All curves are calculated using  $\tau_i = 5.0$ ,  $d_0 = 0.3$ .

Remarkably, it shows pronounced valleys at the magnetic field values of the CPs in  $R_{xx}$  as shown in panel b for the billiard model. In the whole  $B$  range  $\kappa$  is comparable with  $\tau_i$  and even smaller at the commensurable fields. The valleys in  $\kappa(B)$  are the origin of the CPs. It is intuitive that more frequent collisions lead to reduced conductivity and thus increased  $R_{xx}$ . We will confirm this argument below using a simplified stochastic model.

But first we study the structure of  $\kappa(B)$  in more detail. It is not simply a numerical observation, but it has a deep connection with the mixed nature of the phase-space: indeed Fig. 4a clearly shows that it is directly proportional to the measure of the chaotic part of phase space  $g_c(B)$ .

We can understand this striking fact using Kac’s lemma [21–24], which is a direct consequence of phase space volume conservation in Hamiltonian systems. It states that the mean recurrence time  $\mathcal{T}_{\mathcal{S}}$  to a compact subset  $\mathcal{S}$  of the phase space  $\mathcal{M}$  is given by

$$\mathcal{T}_{\mathcal{S}}(B) = \frac{\mu(\mathcal{M}_{acc}; B)}{\mu(\mathcal{S}; B)}, \quad (6)$$

where  $\mu(\cdot)$  is the phase space measure and  $\mathcal{M}_{acc}$  the part of the phase-space accessible to orbits starting in  $\mathcal{S}$  (we have already included the magnetic field dependence for convenience).

Let  $\mathcal{W}$  be a circle of radius  $d_0/2 + \varepsilon$  concentric to the antidot. Implying the limit  $\varepsilon \rightarrow \infty$ , we define  $\mathcal{S} \subset \mathcal{M}$  such that

$$\mathcal{S} = \{\vec{r}, \vec{v} : \vec{r} \in \mathcal{W} \text{ and } \vec{v} \cdot \vec{\eta}(\vec{r}) < 0\} \quad (7)$$

where  $\vec{\eta}(\vec{r})$  is the vector normal to  $\mathcal{W}$  and  $|\vec{v}| = 1$ . The mean collision time  $\kappa$  of the PBS is exactly the mean recurrence time of the set  $\mathcal{S}$  (at  $\varepsilon \rightarrow 0$ ).

To find  $\mu(\mathcal{S}; B)$  we first realize that it does not depend on the magnetic field, i.e.  $\mu(\mathcal{S}; B) = \mu(\mathcal{S}; 0) = \mu(\mathcal{S})$ . Then, using (6) at  $B = 0$ , we have  $\mu(\mathcal{S}) = \mu(\mathcal{M}_{acc}; 0)/\mathcal{T}_{\mathcal{S}}(0)$ . As the PSB without magnetic field is fully ergodic,  $\mu(\mathcal{M}_{acc}; 0) = \mu(\mathcal{M}) = 1$ , and by substitution  $\mathcal{T}_{\mathcal{S}}(B) = \mu(\mathcal{M}_{acc}; B) \times \mathcal{T}_{\mathcal{S}}(0)$ . For small enough magnetic fields all chaotic orbits (and up to measure 0 only those) collide with the antidots. Therefore we have  $\mu(\mathcal{M}_{acc}) \rightarrow g_c$  and  $\mathcal{T}_{\mathcal{S}} \rightarrow \kappa$  and we find

$$\kappa(B) = g_c(B) \times \kappa_0. \quad (8)$$

Thus, the mean collision time is given by the fraction of chaotic orbits as a function of the magnetic field  $B$ , times the mean collision time at  $B = 0$ .

From this derivation it becomes also clear that the collision times are not sensitive to boundary roughness, which is intuitive since the dynamics is already highly chaotic. We confirm that this manifests in magneto-transport by simulating a *rough* periodic Sinai billiard (RPSB) where the particle gets reflected in a random angle at collision with the antidot, corresponding to strong boundary roughness. The changes in the magneto-resistivity are indeed only small as shown in Fig. 4b. To conclude that CPs can be well understood already from the chaotic collision times in the antidot lattice we compare these results to a simple purely stochastic model of the collision events (where only the distribution of the collision times enters in a stochastic renewal process). In every collision the particle is scattered by a randomly orientated wall segment and in-between collisions it performs free cyclotron motion. The calculations are straight forward and are presented in the appendix. This stochastic model reproduces the contribution of the chaotic orbits to the CPs in the RPBS indeed in very good approximation and captures its essence, as shown in Fig. 4c.

In conclusion, we have numerically reproduced recent magneto-transport experiments on graphene antidot lattices using appropriate quasi-classical electron dynamics. We found that ballistic transport features are visible in the resistivities even though the mean free time due to impurity scattering is so short that it is comparable to the fastest timescales of the chaotic dynamics! We showed that this striking robustness of the commensurability features can be understood by the fact that the fast chaotic time scale, the collision time, is reduced by the mere existence of nonlinear resonances due to the reduction of the chaotic phase space volume. In this way we have resolved a long standing controversy on the influence of nonlinear resonances on magneto-transport.

We thank Andreas Sandner and Jonathan Eroms very much for granting us access to their experimental data

and fruitful discussions. We thank Stephan Eule for helpful discussions.

### Stochastic Model

In this appendix we want to derive the expressions for the velocity correlation functions (and thus the resistivities) of the simplified stochastic model for the dynamics in the rough periodic Sinai billiard (RPSB) introduced in the manuscript. We approximate the dynamics by a renewal process of stochastic scattering events (the distribution of the scattering times reflects the geometry of the antidot lattice) and free cyclotron motion in between scattering events. Each scattering event with a rough boundary leads to a random change in the velocity angle

$$\alpha = \pi + 2\psi,$$

where  $\psi$  is the random angle formed by the normal of the boundary segment and the velocity vector of the trajectory undergoing the scattering event. Under the assumption that all spatial orientations of the boundary segments are equally probable the probability density of hitting a segment with angle  $\psi$  is

$$h(\psi) = \frac{1}{2} \cos \psi, \text{ with } \psi \in [-\pi/2, \pi/2]. \quad (9)$$

The correlation functions are

$$C_{xx} = \langle v_y(t)v_x(0) \rangle = v_0^2 \langle \cos(\varphi(t)) \cos(\varphi(0)) \rangle \quad (10)$$

$$C_{yx} = \langle v_y(t)v_x(0) \rangle = v_0^2 \langle \sin(\varphi(t)) \cos(\varphi(0)) \rangle, \quad (11)$$

where  $v_0$  is the constant absolute value of the velocity and the ensemble average  $\langle \cdot \rangle$  reduces to an average over the initial angle  $\varphi_0$  of the velocities and the collision events. In the free propagation in-between events the velocity angle changes by  $\Delta\varphi(t) = \omega\Delta t$ , where the cyclotron frequency  $\omega$  in our units is given by  $\omega = 2B$ . The contribution to the correlation functions of all trajectories that have scattered (exactly)  $m$  times up to time  $t$  is given by

$$C_{xx}(t|m) = P_m(t; B) \int_{-\pi}^{\pi} d\varphi_0 \int_{-\pi/2}^{\pi/2} d\psi_1 \cdots \int_{-\pi/2}^{\pi/2} d\psi_m \frac{\cos \varphi_0}{2\pi} \cos \left( \omega t + \varphi_0 + m\pi + 2 \sum_{i=1}^m \psi_i \right) \frac{\prod_{i=1}^m \cos \psi_i}{2^m} \quad (12)$$

$$C_{yx}(t|m) = P_m(t; B) \int_{-\pi}^{\pi} d\varphi_0 \int_{-\pi/2}^{\pi/2} d\psi_1 \cdots \int_{-\pi/2}^{\pi/2} d\psi_m \frac{\cos \varphi_0}{2\pi} \sin \left( \omega t + \varphi_0 + m\pi + 2 \sum_{i=1}^m \psi_i \right) \frac{\prod_{i=1}^m \cos \psi_i}{2^m}, \quad (13)$$

where  $P_m(t; B)$  is the probability that a trajectory has scattered exactly  $m$  times up to time  $t$ . The  $\psi_i$  integrals can be easily carried out successively. Using the notation  $\phi_m = \omega t + \varphi_0 + m\pi + 2 \sum_{i=1}^m \psi_i$ , we write

$$\begin{aligned} \cos(\phi_m) &= \cos(\phi_{m-1} + 2\psi_m) \\ &= \cos(\phi_{m-1}) \cos(2\psi_m) - \sin(\phi_{m-1}) \sin(2\psi_m) \end{aligned}$$

and

$$\sin(\phi_m) = \cos(\phi_{m-1}) \sin(2\psi_m) + \sin(\phi_{m-1}) \cos(2\psi_m).$$

With

$$\begin{aligned} \frac{1}{2} \int_{-\pi/2}^{\pi/2} \cos(x) \cos(2x) dx &= \frac{1}{3}, \\ \frac{1}{2} \int_{-\pi/2}^{\pi/2} \cos(x) \sin(2x) dx &= 0 \end{aligned}$$

and

$$\frac{1}{2\pi} \int_{-\pi}^{\pi} \cos(\varphi_0) \cos(\omega t + \varphi_0) d\varphi_0 = \frac{1}{2} \cos(\omega t)$$

we find  $C_{xx}(t|m) = \frac{1}{2} (-\frac{1}{3})^m \cos(\omega t)$  and  $C_{yx}(t|m) = \frac{1}{2} (-\frac{1}{3})^m \sin(\omega t)$ . This finally allows us to write the correlation functions as the sum of these contributions:

$$C_{xx}(t) = \frac{v_0^2}{2} \sum_{m=0}^{\infty} \left(-\frac{1}{3}\right)^m P_m(t; B) \cos(\omega t) \quad (14)$$

$$C_{yx}(t) = \frac{v_0^2}{2} \sum_{m=0}^{\infty} \left(-\frac{1}{3}\right)^m P_m(t; B) \sin(\omega t). \quad (15)$$

The probability density function (pdf) of the collision time  $p(t)$  is a complicated function that is very sensitive to changes in the magnetic field, as shown in Fig. 5. Therefore it is hard to find a useful analytical model for the probability  $P_m(t; B)$ . Only in the limit of large  $m$  they are well approximated by Gaussians (see e.g. [25]). We are, however, mainly interested in short times and thus small  $m$ . Therefore we choose to calculate the  $P_m(t; B)$  numerically using the following method: let  $q_m(t)$  denote the pdf for the  $m$ -th scattering event ( $m \geq 1$ ) occurring at time  $t$ . It can be calculated through

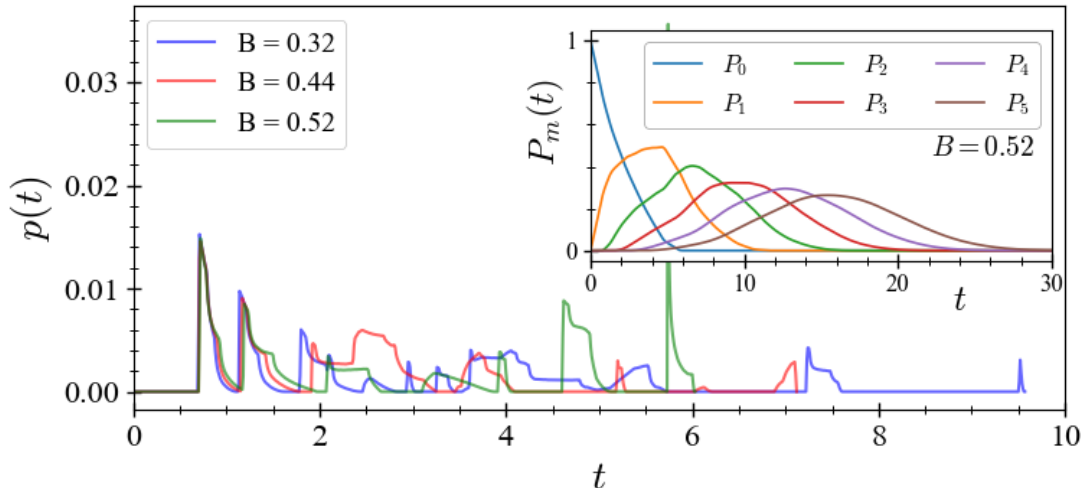


FIG. 5. Probability density function of the collision times  $p(t_n)$  in the rough periodic Sinai billiard for the magnetic fields values marked by black stars in Fig. 4 of the manuscript, i.e.  $B \in \{0.32, 0.44, 0.52\}$ . The inset shows numerically computed probabilities  $P_m(t; B)$  for  $B = 0.52$ .

recursive convolution with the pdf  $p(t)$ ,

$$q_m(t) = \int_0^t dz p(z)q_{m-1}(t-z)$$

with  $q_1(t) \equiv p(t)$ . Then  $P_m(t)$  can be found from  $q_m$  using the survival function  $W(t) = \int_t^\infty p(t')dt'$

$$P_m(t) = \int_0^t dz W(z)q_m(t-z) \quad (16)$$

for  $m > 0$  and  $P_0(t) \equiv W(t)$ . Examples of  $P_m(t)$  are shown in the inset of Fig. 5. Finally, using the Kubo-formula (Eq. 2 and 3 of the manuscript) with impurity scattering time  $\tau_i = 5$  we obtain the magneto-resistance curve shown in Fig. 4 of the manuscript, which clearly demonstrates that the main contribution to the commensurability peaks is already captured by this simple model.

---

[1] K. Ensslin and P. M. Petroff, Phys. Rev. B **41**, 12307 (1990).  
 [2] D. Weiss, M. L. Roukes, a. Menschig, P. Grambow, K. Von Klitzing, and G. Weimann, Phys. Rev. Lett. **66**, 2790 (1991).  
 [3] A. Lorke, J. P. Kotthaus, and K. Ploog, Phys. Rev. B **44**, 3447 (1991).  
 [4] See e.g. ZL. Xiao *et al.* Appl. Phys. Lett. **81**, 2869 (2002); R. Wordenweber *et al.*, Phys. Rev. B **69**, 184504 (2004); S. Neusser *et al.* Phys. Rev. B **78**, 054406 (2008).  
 [5] A. Sandner, T. Preis, C. Schell, P. Giudici, K. Watanabe, T. Taniguchi, D. Weiss, and J. Eroms, Nano Lett. **15**, 8402 (2015).

[6] R. Yagi, R. Sakakibara, R. Ebisuoka, J. Onishi, K. Watanabe, T. Taniguchi, and Y. Iye, Phys. Rev. B (2015).  
 [7] D. Weiss, K. Richter, A. Menschig, R. Bergmann, H. Schweizer, K. von Klitzing, and G. Weimann, Phys. Rev. Lett. **70**, 4118 (1993).  
 [8] H. Silberbauer and U. Rossler, Phys. Rev. B **50** (1994).  
 [9] K. Richter, Europhys. Lett. **29**, 7 (1995).  
 [10] R. Fleischmann, T. Geisel, and R. Ketzmerick, Phys. Rev. Lett. **68**, 1367 (1992).  
 [11] W. Kang, H. L. Stormer, L. N. Pfeiffer, K. W. Baldwin, and K. W. West, Physica B **211**, 396 (1995).  
 [12] R. Fleischmann, T. Geisel, C. Holzknicht, and R. Ketzmerick, Europhys. Lett. **36**, 167 (1996).  
 [13] É. Baskin, G. Gusev, Z. Kvon, A. Pogosov, and M. Entin, JETP Lett. **55**, 678 (1992).  
 [14] R. Schuster, G. Ernst, K. Ensslin, M. Entin, M. Holland, G. Böhm, and W. Klein, Phys. Rev. B **50**, 8090 (1994).  
 [15] M. Fließner, G. J. O. Schmidt, and H. Spohn, Phys. Rev. E **53**, 5690 (1996).  
 [16] S. Ishizaka and T. Ando, Phys. Rev. B **55**, 16331 (1997).  
 [17] We have numerically confirmed that including stochastic scattering in the dynamics gives the same result as the exponential dampening of eq. (2), even in the case of small angle scattering, where  $\tau_i$  has to be regarded as the *transport mean free time*.  
 [18] V. I. Arnold, *Mathematical Methods of Classical Mechanics*, Graduate Texts in Mathematics, Vol. 60 (Springer New York, New York, NY, 1989).  
 [19] We developed our own open-sourced software package to simulate the periodic Sinai billiard in a magnetic field: [github.com/JuliaDynamics/DynamicalBilliards.jl](https://github.com/JuliaDynamics/DynamicalBilliards.jl).  
 [20] Y. G. Sinai, Russ. Math. Surv. **25**, 137 (1970).  
 [21] M. Kac, Bull. Amer. Math. Soc **20**, 376 (1947).  
 [22] R. S. MacKay, Journal of Nonlinear Science **4**, 329 (1994).  
 [23] J. D. Meiss, Chaos **7**, 139 (1997).

- [24] E. G. Altmann and T. Tel, *Phys. Rev. Lett.* **100**, 1 (2008).
- [25] K. V. Mitov and E. Omev, *Renewal Processes* (Springer International Publishing, 2014).